19th International Conference
ENGINEERING MECHANICS 2013
Svratka, Czech Republic, May 13 – 16, 2013

EXPERIMENTAL VERIFICATION OF RESONANCE BEHAVIOUR OF A DAMPED SPHERICAL PENDULUM

C. Fischer, S. Pospíšil, J. Náprstek [1]

Summary: *Theoretical, experimental and numerical analysis of a spherical pendulum is carried out. The stability of the response in a vertical plane is analysed in the theoretically predicted resonance region. Mathematical model respects the non-linear character of the pendulum and allows to introduce asymmetrical damping. Experimental analysis is performed using a special experimental frame where a pendulum is supported by the Cardan joint and damped by two magnetic units. Uni-directional harmonic excitation is applied to the system. These units are able to reproduce linear viscous damping independently in both principal response components. Measured data are compared to theoretical and numerical results.*

Keywords: ***non-linear vibration, experimental verification, viscose damping, spherical pendulum, autoparametric system***

1. Introduction

Many civil engineering structures are equipped by tuned mass dampers (TMDs). These devices are designed to draw away vibrational energy from the structure and dissipate it internally, reducing the undesired response. In case of tall structures the typical TMD has a form of a heavy pendulum placed close to the top of the structure. Such devices are very popular for their reliability and simple maintenance, see e.g. (Haxton, 1974; Náprstek & Pirner, 2002). Dynamic behaviour of such a substructure is however significantly more complex than it is supposed by widely used simple linear single degree-of-freedom (SDOF) models working in a vertical plane only. Such a linear model is satisfactory only if the amplitude of kinematic excitation at the suspension point is very small and if its working frequency remains outside of a resonance frequency domain which is possible only at the cost of lower efficiency of the damper. Moreover, the typical installation differs significantly of the idealized model of a pendulum. The bob can be suspended on chains, sometimes from several hinges. Damping of the bob is usually realized by installing oil dampers in certain directions only. The presented theoretical and experimental models comprise such properties up to certain level.

In the experimental as well as in numerical treatment an uni-directional harmonic excitation is supposed. If the excitation frequency belongs to the resonance region, post-critical states can emerge. These states are characterized by either highly increased in-plane response, or by more or less complicated space trajectories of various types. From the practical point of view, such a type of the response destroys effectiveness of the TMD.

[1] RNDr. Cyril Fischer, Ph.D., doc. ing. Stanislav Pospíšil, Ph.D., Ing. Jiří Náprstek, DrSc., Institute of Theoretical and Applied Mechanics, Prosecká 76, 190 00 Prague 9, tel. +420 286 88 21 21, e-mail FischerC@itam.cas.cz

The horizontally forced spherical pendulum was first studied by Miles (1962), who considered the problem of the stability of planar oscillations to non-planar perturbations for small amplitude forcing in the neighbourhood of resonance using truncated equations. He found that planar solutions become sensitive to non-planar perturbations in particular parameter ranges and that there arise also non-planar oscillations. Later on, a more detailed study by the same author (Miles, 1984) analysed a set of bifurcation diagrams for planar and non-planar motions as well as chaotic motion. The experiments carried out by Tritton (1986) in the same topic approved the theoretical model and showed good agreement with the theoretical results.

The presented work is an extension of the article which has been published by the authors recently in (Pospíšil et al., 2012) and (Fischer et al., 2012) with the focus put upon the influence of uneven damping in individual directions on the overall stability. Movement of the pendulum is described analytically using the approach by Náprstek & Fischer (2009), the derived equations are treated analytically and numerically.

In the experimental part of the paper, the problem is examined using a specially developed experimental rig. It contains kinematically driven pendulum suspended at a Cardan joint. The response components are measured by the rotation sensors. The key parameter, damping, can be adjusted for each response component by means of two independent magnetic units attached to the frame and to the supporting axes of rotation. These units are able to reproduce the linear viscous damping.

2. Theoretical and numerical model

The spherical pendulum is modelled as a strongly non-linear dynamic system with kinematic external excitation in the suspension point, see Figure 1.

The mathematical model follows from the balance of kinetic and potential energies. The expression for kinetic and potential energies T, V in the Cartesian system $(\xi = \xi(t), \zeta = \zeta(t), \eta = \eta(t))$ can be expressed in the following form:

$$T = \frac{m}{2}(\dot{\xi}^2 + \dot{\zeta}^2 + \dot{\eta}^2 + 2\dot{a}\dot{\xi} + \dot{a}^2) \qquad (1)$$

$$V = mg\eta \qquad (2)$$

The equations (1-2) should be completed by a following kinematic constraint:

$$r^2 = \xi^2 + \zeta^2 + (r - \eta)^2 \qquad (3)$$

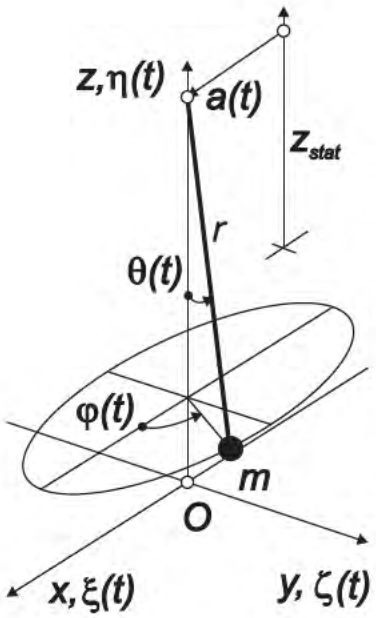

Figure 1: Outline of the idealized model

The geometry of the model is illustrated in Figure 1. The vertical coordinate η starts in the lower pole of the sphere. Parameters m, r are mass and suspension length of the pendulum, respectively, g is the gravitational acceleration and $a(t)$ stands for the external excitation. The detailed derivation of the equations of the mathematical model has been presented by the authors in (Náprstek & Fischer, 2009) and will not be repeated here.

The linear damping proportional to the response velocity will be included by means of the quadratic Rayleigh dissipative function:

$$F = \frac{1}{2} m r^2 \left(\beta_\xi \dot{\xi}^2 + \beta_\zeta \dot{\zeta}^2 + \beta_\eta \dot{\eta}^2 \right) \tag{4}$$

where $\beta_\xi, \beta_\zeta, \beta_\eta$ are the coefficients of viscous damping in individual response components. However, due to the nature of the problem, the damping in the vertical direction will not be taken into account ($\beta_\eta = 0$).

The final approximate Lagrangian system can be obtained after application of the Hamilton's principle (see (Náprstek & Fischer, 2009) for derivation)

$$\left.\begin{aligned} \ddot{\xi} + \frac{1}{2r^2}\xi \frac{\mathrm{d}^2}{\mathrm{d}t^2}(\xi^2 + \zeta^2) + 2\beta_\xi \dot{\xi} + \omega_0^2 \left(\xi + \frac{1}{2r^2}\xi(\xi^2 + \zeta^2) \right) &= -\ddot{a} \qquad (a) \\ \ddot{\zeta} + \frac{1}{2r^2}\zeta \frac{\mathrm{d}^2}{\mathrm{d}t^2}(\xi^2 + \zeta^2) + 2\beta_\zeta \dot{\zeta} + \omega_0^2 \left(\zeta + \frac{1}{2r^2}\zeta(\xi^2 + \zeta^2) \right) &= 0 \qquad (b) \end{aligned}\right\} \tag{5}$$

Natural frequency of the corresponding linear pendulum is given by $\omega_0^2 = g/r$. The equations (5) are mutually independent if only linear terms are taken into account.

Assuming the harmonic excitation $a(t) = a_0 \sin \omega t$ and semi-trivial solution in the form of (see e.g. (Tondl, 1991) for details)

$$\xi_0 = a_c \cos \omega t + a_s \sin \omega t \; ; \;\; \zeta_0 = 0 \tag{6}$$

expression for the non-linear resonance curve of the amplitude of the response ($R_0^2 = a_c^2 + a_s^2$) can be found as follows:

$$R_0^2 \left[4\omega^2 \beta_\xi^2 + \left((\omega^2 - \omega_0^2) + \frac{R_0^2}{2r^2} \left(\omega^2 - \frac{3}{4}\omega_0^2 \right) \right)^2 \right] - 4\omega^4 a_0^2 \; = \; 0 \tag{7}$$

Limits of the semi-trivial solution stability (or validity) modified for the case of distinct damping coefficients in the individual directions are as follows:

$$\frac{3R_0^4 \left(\omega^2 - \frac{3\omega_0^2}{4} \right)^2}{4r^4} + \frac{2R_0^2 \left(\omega^2 - \omega_0^2 \right) \left(\omega^2 - \frac{3\omega_0^2}{4} \right)}{r^2} + \left(\omega^2 - \omega_0^2 \right)^2 + 4\omega^2 \beta_\xi^2 = 0 \tag{8}$$

$$\frac{R_0^4 \left(\omega^2 + \frac{\omega_0^2}{4} \right) \left(\frac{3\omega_0^2}{4} - \omega^2 \right)}{4r^4} + \frac{R_0^2 \omega_0^2 \left(\omega_0^2 - \omega^2 \right)}{2r^2} + \left(\omega^2 - \omega_0^2 \right)^2 + 4\omega^2 \beta_\zeta^2 = 0 \tag{9}$$

Derivation of (8-9) follows the same procedure like in the case for $\beta_\xi = \beta_\zeta$. Figure 2 shows configuration of the resonance curve and both stability limits for several values of in-plane and out-of-plane damping coefficients. It can be seen that the stability of the semi-trivial solution is more sensitive to the damping coefficient in the out-of-plane direction (β_ζ) — the semi-trivial solution loses its validity even for relatively high values of damping coefficient.

If a more general form of the stationary solution is assumed, namely

$$\xi(t) = a_c \cos \omega t + a_s \sin \omega t \; ; \qquad \zeta(t) = b_c \cos \omega t + b_s \sin \omega t \tag{10}$$

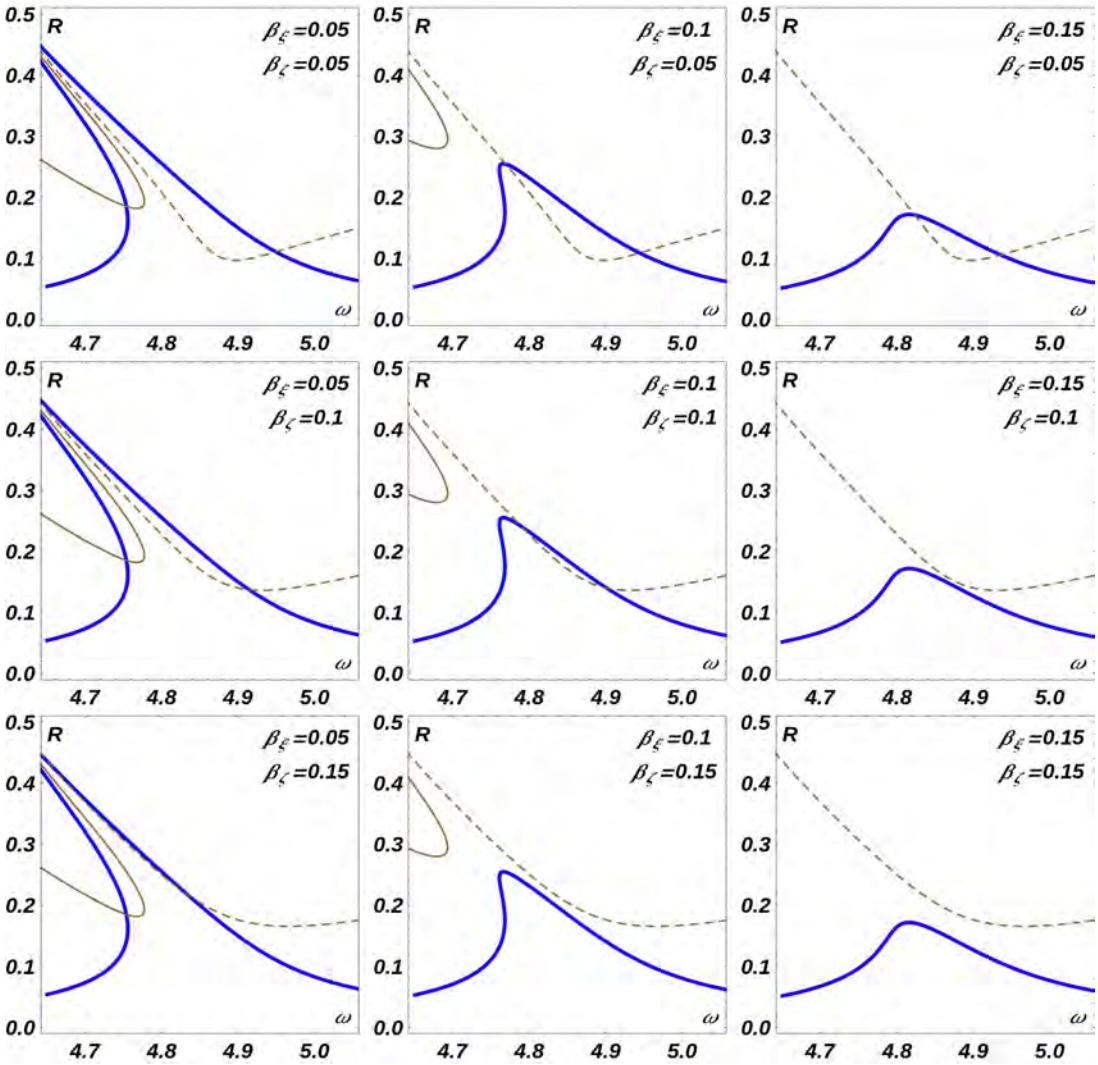

Figure 2: Resonance curve (thick solid line) and in-plane (ξ - solid) and out-of-plane (ζ - dashed) stability limits of the semi-trivial solution for varying configuration of $\beta_\xi, \beta_\zeta \in \{0.05, 0.1, 0.15\}$. For each plot, on the horizontal axis is excitation frequency ω, on the vertical axis is the amplitude $R = R_0$.

the resonance curve of the semi-trivial solution (7) will be augmented by branches corresponding to the spatial movement. Formulation for the case when the both damping coefficients are the same ($\beta_\xi = \beta_\eta$) has been published previously, see (Náprstek & Fischer, 2009). For the case $\beta_\xi \neq \beta_\eta$ the generalized resonance curve has a more complicated form:

$$\begin{aligned} &-64P^2r^2S^2\omega\Omega_4\left(\beta_\xi-\beta_\zeta\right)+256r^4\omega^2\left(\beta_\xi^2R_0^2+\beta_\zeta^2R_1^2\right)- \\ &\quad -8S^4\Omega_4\left(8r^2\Omega_2+R^2\Omega_1\right)+R^4\left(8r^2\Omega_2+R^2\Omega_1\right)^2+4R^2S^4\Omega_4^2 \;\; = 64r^4a_0^2\omega^4 \end{aligned} \tag{11}$$

$$\begin{aligned} &16P^2r^2\omega\left(8r^2\Omega_2+R^2\Omega_1\right)\left(\beta_x-\beta_y\right)+256r^4\omega^2\beta_x\beta_yS^2+ \\ &\quad +S^2\left(\left(8r^2\Omega_2+R^2\Omega_1\right)^2-2R^2\Omega_4\left(8r^2\Omega_2+R^2\Omega_1\right)+4S^4\Omega_4^2\right) \;\; = 0 \end{aligned} \tag{12}$$

Here $R_0^2 = \left(a_c^2 + a_s^2\right), R_1^2 = \left(b_c^2 + b_s^2\right);\ R_0^2 + R_1^2 = R^2;\ S^2 = a_sb_c - a_cb_s;\ P^2 = a_cb_c + a_sb_s$ and $\Omega_1 = 3\omega_0^2 - 4\omega^2\ ;\ \Omega_2 = \omega_0^2 - \omega^2\ ;\ \Omega_3 = \omega_0^2 + 4\omega^2\ ;\ \Omega_4 = \omega_0^2 - 4\omega^2$. It can be easily

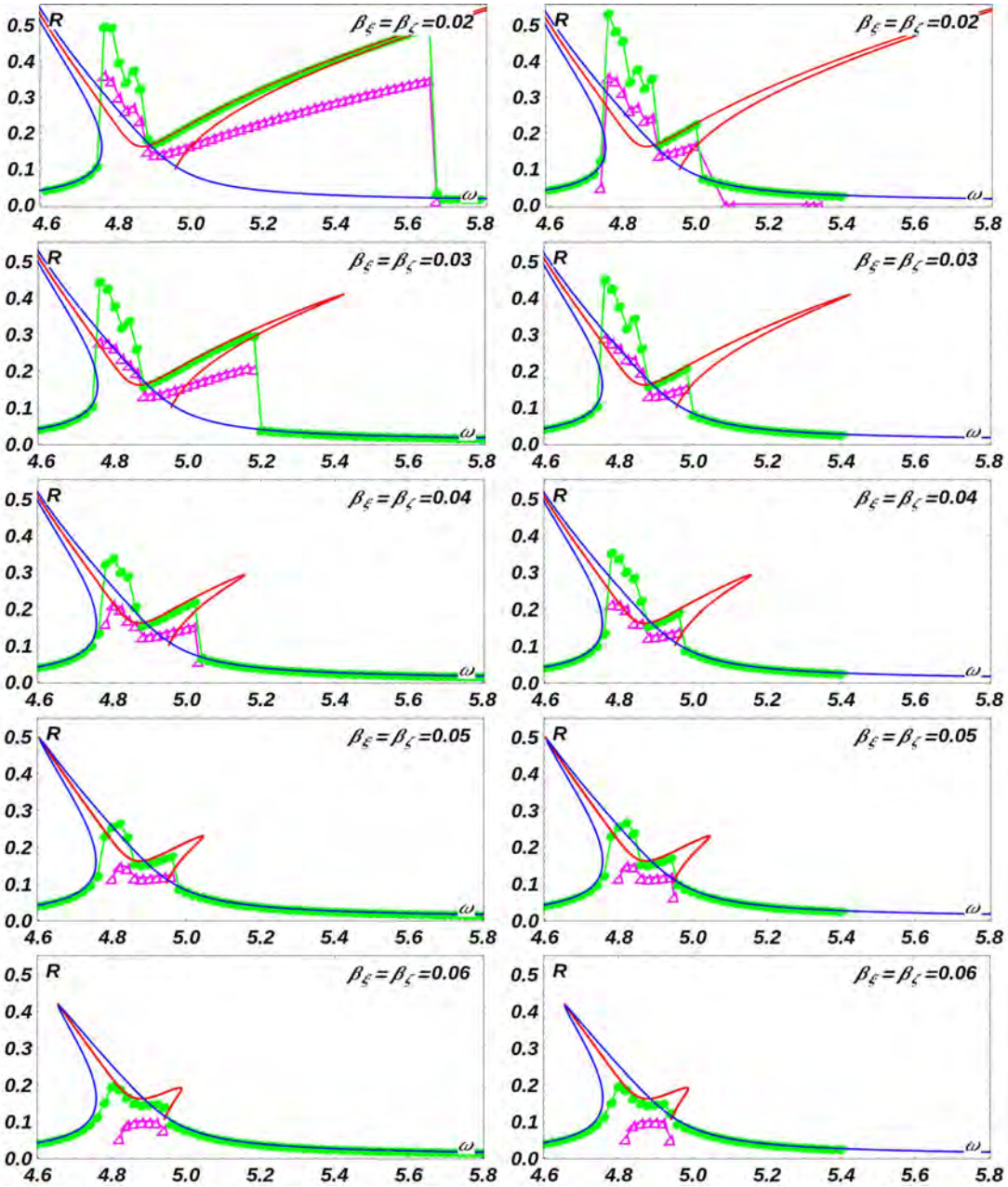

Figure 3: Resonance plot for the more general solution (10). The solid blue and red curves stand for the semi-trivial resonance curve and the $S \neq 0$ branch. The green (bullets) and magenta (triangles) lines correspond to the numerically computed maximal total amplitudes ($\sqrt{\xi^2 + \zeta^2}$) and out-of-plane amplitudes (ζ) respectively. Left column: numerical resonance is computed for continuously varying excitation frequency. Right column: independent computation of the maximal amplitude for each excitation frequency. For each plot, on the horizontal axis is the excitation frequency ω and on the vertical axis is the amplitude $R = \sqrt{R_0^2 + R_1^2}$.

seen, that setting $\beta_\xi = \beta_\eta = \beta$ in equations (11-12) the terms involving P become zero and original equations published in (Náprstek & Fischer, 2009) will be restored. However, the both first terms in (11-12) introduce a new parameter P^2 into the expressions and this makes the both conditions less transparent and usable.

It should be noticed here, that if the semi-trivial solution (12) is valid (i.e. $S = 0$), the equation (11) reduces itself to the resonance curve (7). In the opposite case a new branch appears in the resonance plot which corresponds to the spatial movement of the pendulum. It starts from the spike of the semi-trivial resonance curve, crosses it from below and ends again on the original resonance curve, forming three bifurcation points. Stability of the individual branches can be checked using the Jacobi determinant of the differential system. The resonance plot is depicted in the Figure 3 for several values of damping $\beta_\xi = \beta_\eta = \beta \in 0.02, .., 0.06$. Solid blue and red curves stand for the semi-trivial resonance curve and the $S \neq 0$ branch. The green (bullets) and magenta (triangles) lines correspond to the numerically computed maximal total amplitudes ($\sqrt{\xi^2 + \zeta^2}$) and out-of-plane amplitudes (ζ) respectively.

The both columns in Figure 3 show limited stability of the upper part of the $S \neq 0$ resonance branch. Numerical simulation shows that if the excitation frequency increases slowly during simulation the numerical solution of the system (5) is able to keep the spatial character and to follow the upper part of the $S \neq 0$ resonance branch for a certain number of excitation frequencies (see left column of Figure 3). On the other hand, it is almost impossible to reach this state without knowledge of the exact initial conditions. The numerical resonance curves in the right column of Figure 3 were computed independently for each single excitation frequency and using prescribed fixed initial conditions. The same result can be obtained if random initial conditions are used.

3. Experimental model

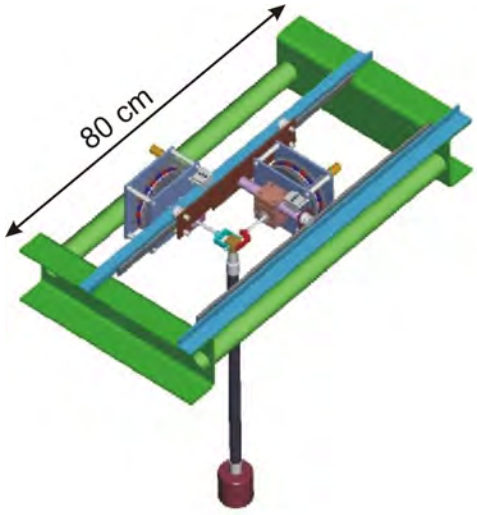

Figure 4: Experimental pendulum

For the experimental evaluation and verification of the above described theory the authors use an experimental pendulum, designed to comply with the assumptions of the theoretical and numerical model. This pendulum is suspended at Cardan joint attached to a trolley to assure uni-directional excitation, see see in Figure 4. The length of the pendulum is 0.41 m, mass of its bob was relatively high to increase inertia and thus to lower structural damping. Fundamental eigenfrequency of the pendulum was measured as $f_0 = 0.76$ Hz, i.e. $\omega_0 = 4.8$ rad $\cdot$ s^{-1}. Response of the pendulum was measured for excitation frequencies ranging from $f_l = 0.7$ Hz to $f_u = 1.1$ Hz with increments $\Delta f = 0.01$ Hz, (i.e. range $\omega = 4.40 \ldots 6.91$ rad $\cdot$ s^{-1}). To cover the full range of the resonance interval, the each sweep was started for excitation frequency slightly higher than the eigenfrequency of the pendulum and small initial disturbance was given to the bob. Then was the excitation frequency gradually changed in small increments up or down to cover the whole frequency range. Each frequency was kept constant for three minutes and angles of the suspender were measured and recorded. To eliminate the transition effects, only the last minute of

each record was taken into account in the post-processing. The same approach has been used in computation of the numerical resonance curve in the left column of Figure 3. Further details of the experimental setup have been published previously in (Pospíšil et al., 2012).

Results of the experimental measurements are summarized in Figures 5–7. Each figure shows experimental and numerical resonance curve for selected values of the damping coefficients. The main part of each figure is the pair of green curves: the dark green thick line corresponds to the maximal total amplitude of the measured response of the experimental pendulum ($\sqrt{\xi^2 + \zeta^2}$). Its numerically computed counterpart is depicted in light green with large bullets. The green curves are repeated in the both figures for ξ and ζ (left and right column). The thin blue and pink curves stand for minimal and maximal amplitudes of the measured time histories of the ξ component in the left column and ζ component on the right. The greyish area between these curves indicates non-stationarity of the response. Thus, if the response is stationary the both curves coincide. The brown curve with small bullets in figures for ξ component (left) and magenta line with triangles in figures for ζ (right) show the numerically computed maxima. The numerical results follow the procedure which have been used for the left column of Figure 3. Finally, each figure is supplemented with the theoretical resonance curve of the corresponding semi-trivial solution (dotted blue) and two stability limits (dashed brown lines).

To comment the Figures 5–7 a few preliminary remarks have to be made. Although Miles (1984) or Náprstek & Fischer (2009) divide the resonance interval in detail, for purpose of

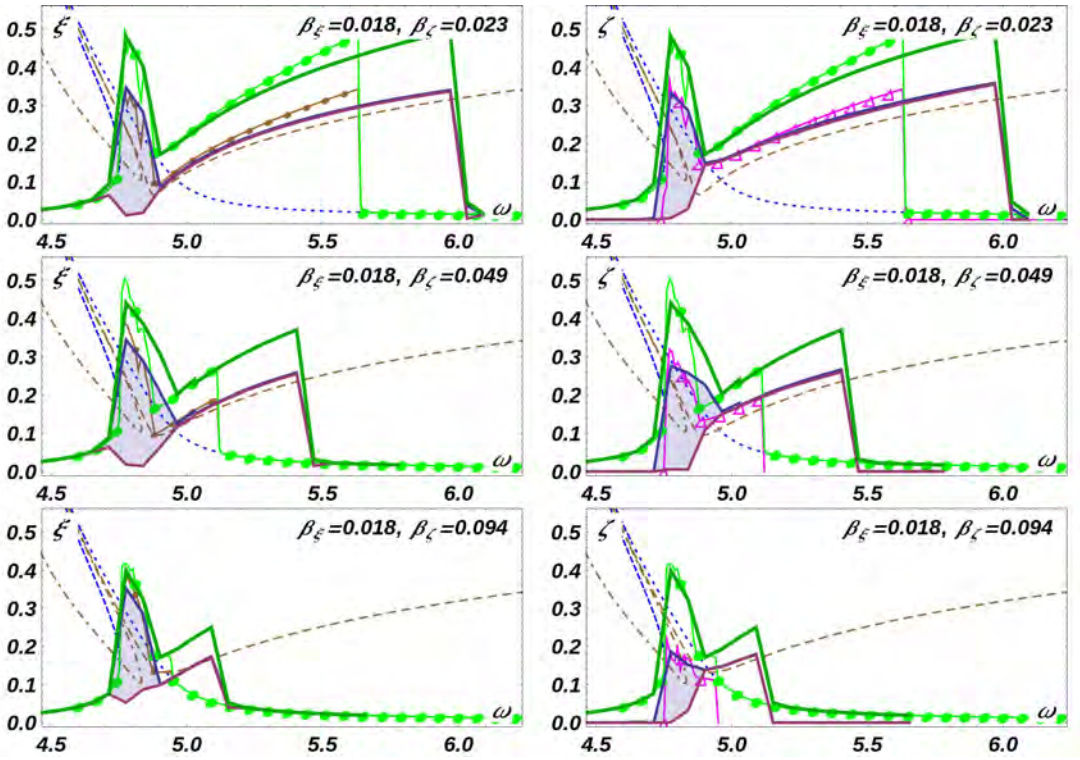

Figure 5: Experimental and numerical resonance plots for $\beta_\xi = 0.018$ and increasing β_ζ. In-plane component (ξ) and total amplitude on the left, out-of-plane movement (ζ) and total amplitude on the right. In Figures 5–7: solid lines – experimental data, solid lines with signs – numerical data, dotted and dased lines – theoretical results, cf. Figure 2. Green – total amplitude R, blue, pink, brown & magenta – component amplitudes (ξ and ζ).

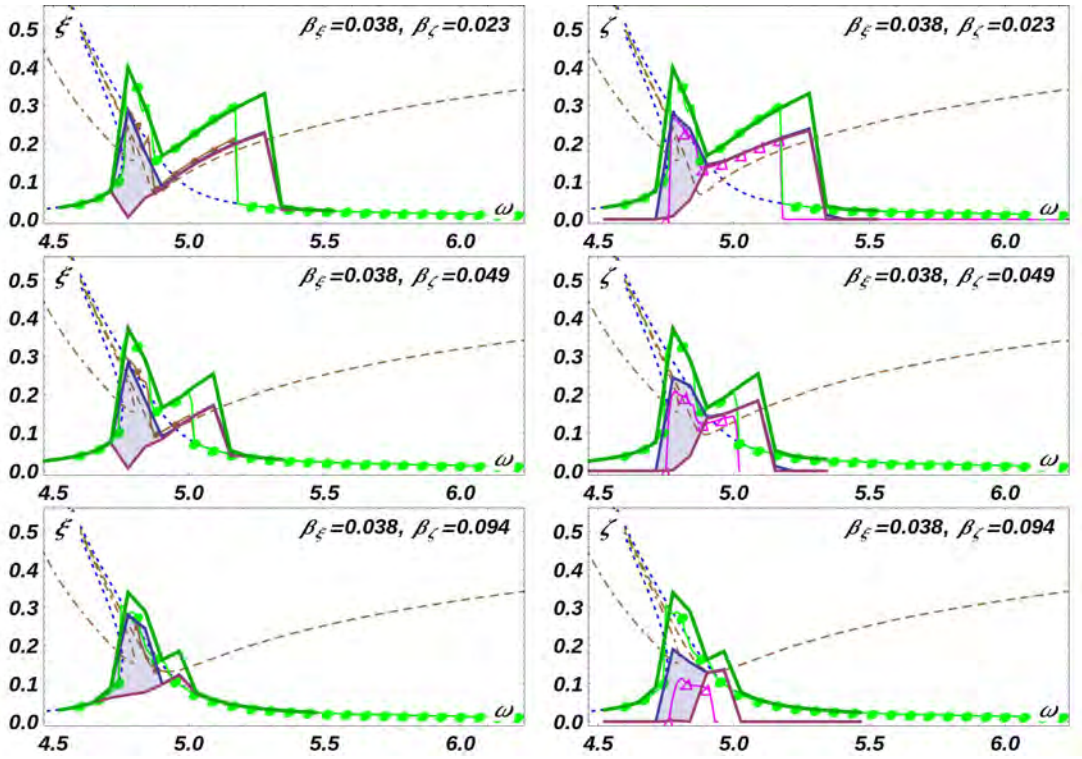

Figure 6: Experimental and numerical resonance plots for $\beta_\xi = 0.038$ and increasing β_ζ. In-plane component (ξ) and total amplitude on the left, out-of-plane movement (ζ) on the right.

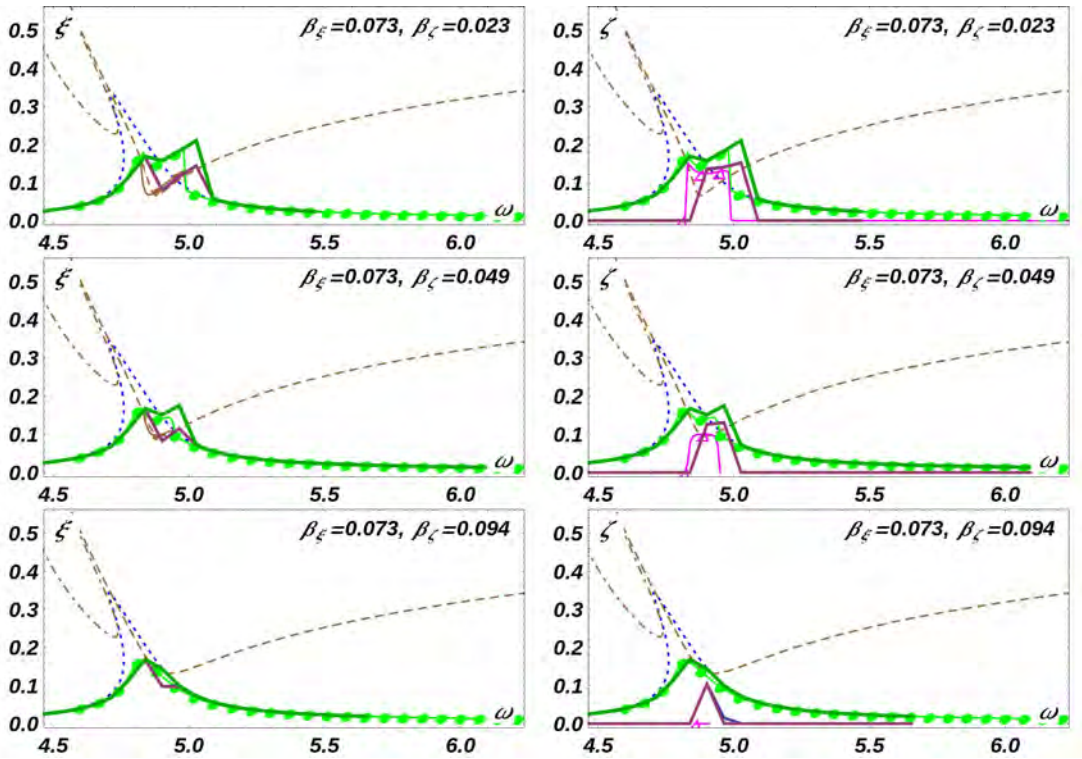

Figure 7: Experimental and numerical resonance plots for $\beta_\xi = 0.073$ and increasing β_ζ. In-plane component (ξ) and total amplitude on the left, out-of-plane movement (ζ) on the right.

this work it is sufficient to distinguish the interval of stationary and non-stationary spatial response, as it is indicated by presence/absence of the greyish area in the resonance plots. The non-stationary response have a form of quasi-periodic or chaotic movement and it will not be commented further. The stationary spatial response is characterised by a movement on an elliptic trajectory. The total amplitude R of the stationary response follows the $S \neq 0$ branch of the resonance curve (11), see the red curves in Figure 2 and namely their increasing part.

The deflection of the numerical and experimental amplitude responses in the stationary part of the resonance interval is not too significant. It follows from the formulation of the approximate mathematical model, which does not comprise dependence of instantaneous frequency on amplitude of the pendulum. On the other hand, the good agreement between numerical and experimental resonance curves in the non-stationary part of the resonance interval is surprising.

In Figure 5 is the in-plane damping set to a low value $\beta_\xi = 0.018$. The correspondence between numerical and experimental resonance curve is rather good. Main difference is in the upper stable branch of the theoretical resonance curve. Despite the fact, that the frequency increment of the experimental case is larger then in the numerical computation (0.01 Hz vs. 0.01 rad.s^{-1} = 0.0016 Hz) the experimental pendulum is able to follow the stable spatial branch significantly longer than the numerical procedure. Exact cause of this difference is unknown.

Increasing β_ζ from 0.023 to 0.094 while keeping $\beta_\xi = 0.018$ reduces the upper end of the resonance interval significantly: from 6.0 to 5.1 rad.s^{-1}. The lower end depends on the value of β_ξ. On the other hand, keeping the β_ζ at a constant value 0.023 and increasing β_ξ to 0.073 eliminates almost completely the non-stationary response and moves the upper end of the resonance interval even lower – to 5.05 rad.s^{-1}, see first lines of Figures 5–7.

A similar conclusions can be drawn if the results shown in individual Figures 5–7 are compared to results in first, second or third row of every Figure 5–7. Increasing β_ξ while β_ζ is kept constant the non-stationary response region fades away and the interval of stationary spatial response reduces its extent. Increasing β_ζ and keeping β_ξ has only marginal influence on the non-stationary response, but significantly reduces the interval of stationary spatial response.

Figure 8 summarizes the maximal amplitudes of the measured response in directions ξ and ζ for individual configurations of damping coefficients β_ξ and β_ζ. It is clear from the left figure

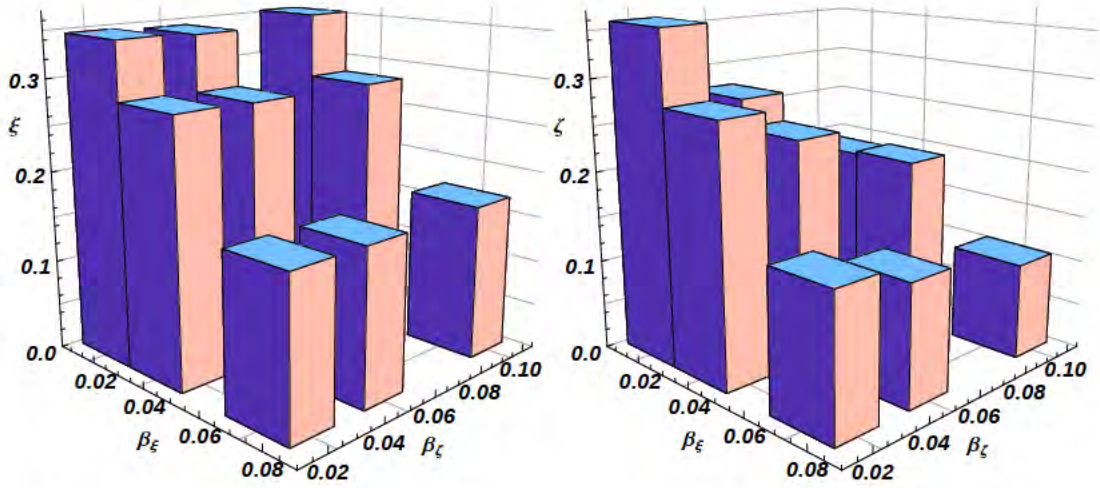

Figure 8: The maximal amplitude of the measured response in ξ (left) and ζ (right) direction for various β_ξ and β_ζ.

that the maximal in-plane response ξ depends mainly on the value β_ξ and influence of β_ζ is negligible. On the other hand, maximal amplitude of the out-of-plane motion depends on both damping coefficients approximately equally.

Data shown in Figure 8 correspond well to the results of the extensive numerical study obtained the authors and presented in Figure 4 in (Fischer et al., 2012). The current experimental data confirm the hypotheses outlined in the last-mentioned work, namely that the occurrence of non-zero out-of-plane motion does not depend significantly on the value of β_ζ.

4. Conclusions

Analytical, experimental and numerical investigation has shown that widely used linear model of the damping pendulum is acceptable only in a very limited extent of parameters concerning pendulum characteristics and excitation properties. A more complicated non-linear model must be introduced for a general analysis.

The results of the experimental and numerical investigation have exhibited a good agreement. Role of the individual damping coefficients β_ξ and β_ζ which has been postulated by the authors in (Fischer et al., 2012) has been confirmed and improved. It has been shown, that initiation of the spatial response is more sensitive to damping in the in-plane direction (β_ξ). The maximal amplitude of the in-plane response exhibits almost no sensitivity to value of the out-of-plane damping (β_ζ). Increasing of the both components β_ξ and β_ζ shorten the resonance interval and diminish the maximal amplitude of the out-of-plane component of the response.

The presented results also respond to some open questions which were left in (Fischer et al., 2012). It has appeared, that the stable branch of the resonance curve corresponding to spatial movement of the pendulum can coexist with a much milder stable planar branch and both branches can be reached numerically and experimentally. On the other hand, the spatial movement is much more sensitive to initial conditions in the both numerical and experimental approach. Surprisingly, the experimental pendulum is able to follow the spatial branch of the resonance curve significantly longer that the numerical procedure does for increasing excitation frequency.

From the practical point of view, it is highly recommended to design the damping pendulum absorber in such a way that any intersections of the resonance curve with the stability limits are avoided. Especially intersection with in-plane (ξ) stability limit should be prevented, otherwise negative influence of the pendulum in the resonance domain is to be expected in both along-wind as well as in cross-wind directions.

5. Acknowledgment

The kind support of the Czech Scientific Foundation No. 103/09/0094, Grant Agency of the ASCR No. A200710902 as well as the support of RVO 68378297 are gratefully acknowledged.

6. References

Fischer, C., Náprstek, J., Pospíšil (2012) Resonance behaviour of spherical pendulum – influence of damping. *Engineering Mechanics 2012*, Náprstek and Fischer (eds), ITAM AS CR, v.v.i., Prague, pp. 255261

Haxton, R. S., Barr, A. D. S. (1974) The autoparametric vibration absorber. *ASME J. Appl. Mech.* 94, pp. 119-125.

Miles, J. W. (1962) Stability of forced oscillations of a spherical pendulum. *Quart. J. Appl. Math.* 20, pp. 21-32.

Miles, J. W. (1984) Resonant motion of spherical pendulum. *Physica D* 11, pp. 309-323.

Náprstek, J., Fischer, C. (2009) Auto-parametric semi-trivial and post-critical response of a spherical pendulum damper. *Comput. Struct.* 87, pp. 1204-1215.

Náprstek, J., Pirner, M. (2002), Non-linear behaviour and dynamic stability of a vibration spherical absorber. In: *Proc. 15th ASCE Engineering Mechanics Division Conference* (A. Smyth et al. eds). Columbia Univ., New York, CD ROM, paper #150, 10 pp.

Pospíšil, S., Fischer, C., Náprstek, J. (2011) Experimental and theoretical analysis of autoparametric stability of pendulum with viscous dampers. *Acta Technica CSAV*, 56, 4, pp. 359–378.

Tondl, A. (1991) *Quenching of Self-Excited Vibrations*, Academia, Prague.

Tritton, D. J. (1986) Ordered and chaotic motion of a forced spherical pendulum, European Journal of Physics. 7, pp. 162–169.